Effect of Grain Size on Magnetic Loss of Nanocrystalline Alloy Under High-Frequency Non-Sinusoidal Excitation

Li Zhang[1], Yifan Wang[1], Liang Zou[1], Kaihang Guo[2], Yongjian Li[3], and Qiuxia Sun[4]

[1]School of Electrical Engineering, Shandong University, Jinan 250061, China
[2]Dalian Power Supply Company of State Grid Liaoning Electric Power Company Ltd., Dalian 116001, China
[3]Key Laboratory of Electromagnetic Field and Electrical Apparatus Reliability of Hebei Province, Hebei University of Technology, Tianjin 300130, China
[4]Shandong Taikai Transformer Company Ltd., Taian 271000, China

To investigate the effects of internal microstructure and high-frequency non-sinusoidal excitation on the magnetic loss of nanocrystalline alloy, a 3-D mesoscopic model based on G. Herzer's theory of random anisotropy is developed. First, the ac test platform is used to measure the loss value of the nanocrystalline alloy under sinusoidal excitation, and then, the model is subjected to the same excitation to obtain its loss value. These values are compared to verify the model's accuracy. Using the micromagnetic model provided by OOMMF software, we investigate the microscopic effect of grain size d on the high-frequency magnetic loss p_v of nanocrystalline alloys. Next, we apply non-sinusoidal alternating magnetic fields (square wave, trapezoidal wave, and triangular wave) to the model to explore p_v under non-sinusoidal excitation. The results show that as the grain size d of the nanocrystalline alloy increases, p_v also increases. Additionally, when d and the frequency f are held constant, p_v is greatest under triangular wave excitation, followed by trapezoidal wave excitation, and smallest under square wave excitation. This conclusion is due to the fact that the equivalent frequency f_{eq}, which contains the rate of change of magnetic flux density (dB/dt), can replace f in the original Steinmetz formula when the excitation source is non-sinusoidal. Our calculations indicate that f_{eq} is smaller under square wave excitation than under triangular wave excitation.

Index Terms— **Grain size, high-frequency magnetic loss, nanocrystalline alloy, non-sinusoidal excitation.**

I. Introduction

With the rapid development of direct current transmission technology and the large-scale integration of renewable energy, the high-frequency transformer has received increasing attention [1], [2], [3], [4]. Compared to power frequency transformers, high-frequency transformers have several advantages, such as a smaller size, higher power density, and constant load-side voltage output. However, high-frequency transformers are also subject to a range of complex operating conditions [5]. The excitation voltage often contains non-sinusoidal waves, such as square waves. These distorted non-sinusoidal waves can cause changes in the microstress inside the core material, including the magnetic domain microstress inside the magnetic powder and the interface microstress between the magnetic powder and the insulation coating layer. This can result in changes in the high-frequency loss of the transformer. Furthermore, as the operating frequency increases steadily to kilohertz, the core loss in the high-frequency magnetic field increases dramatically, placing additional demands on the performance of the core materials for high-frequency transformers [6]. Nanocrystalline alloy is a type of two-phase composite ferromagnetic material, with a microstructure consisting of spherical nanograins scattered throughout the amorphous matrix. This material exhibits outstanding soft magnetic qualities, including high effective permeability, low loss, high saturation magnetic flux density, and low coercivity. Additionally, it is inexpensive, easy to prepare, and highly heat resistant, making it a promising candidate for high-frequency transformer core materials [7], [8], [9], [10].

In recent years, significant advancements have been made by numerous scholars in understanding the magnetic loss and characteristics of nanocrystalline alloy materials. Starodubtsev et al. [11] studied the hysteresis loss of nanocrystalline $Fe_{67.5}Co_5Cu_1Nb_2Mo_{1.5}Si_{14}B_9$ alloy with magnetic field-induced anisotropy and its relationship with small static hysteresis loop parameters. A hysteresis mechanism related to irreversible magnetization rotation in ferromagnetic clusters of nanocrystalline alloys is proposed, and a formula is proposed for calculating the hysteresis loss in soft magnetic nanocrystalline materials with different magnetic anisotropy. In [12], $Fe_{79}Si_9B_{4.5}P_{1.5}CuNb_x$ alloy was prepared by the melt spinning method, and it was found that Nb can reduce the grain size of the alloy. The unit magnetic loss of the alloy with $x = 2$ is 5.84 W/kg, which is 19% lower than that of $x = 1$. Kampen et al. [13] introduced the Grätzer shape factor based on the loss separation theory to improve the Bertotti model, making it suitable for sine wave, triangular wave, and rectangular wave in a wide range of magnetization frequency conditions.

While the aforementioned studies have focused on macroscopic experiments on material preparation processes, they have not been able to fully characterize the changes in internal microstructures of the material or explain the influence of distorted non-sinusoidal alternating magnetic fields on high-frequency magnetic loss. As such, they lack the

Manuscript received 2 February 2023; revised 26 March 2023 and 25 April 2023; accepted 28 April 2023. Date of publication 17 May 2023; date of current version 28 June 2023. Corresponding author: Y. Wang (e-mail: 202234744@mail.sdu.edu.cn).

Color versions of one or more figures in this article are available at https://doi.org/10.1109/TMAG.2023.3277075.

Digital Object Identifier 10.1109/TMAG.2023.3277075

theoretical support required for the application of nanocrystalline alloy in high-frequency transformer cores. To address this gap, Jiale [14] conducted micromagnetic simulations of nanocrystalline alloys and found that the movement of the domain wall lags behind the magnetic moment deflection during magnetization, which suggests that magnetic moment deflection is a significant factor. Additionally, Zhiyun et al. [15] investigated the impact of amplitude or frequency of the external alternating magnetic field on the magnetization process of nanocrystalline alloys by defining "dynamic saturation" and "static saturation."

However, the aforementioned references have only investigated the rotation of the magnetic moment and the movement of the domain wall during the magnetization process of nanocrystalline alloys when external conditions change. It is challenging to characterize the influence mechanism of high-frequency non-sinusoidal excitation and the change of internal grain size of the material on high-frequency magnetic loss, and there is a lack of theoretical support for the application of nanocrystalline alloys to high-frequency transformer cores. First, the excitation voltage and current of high-frequency transformers are typically not standard sine waves but contain a large number of harmonics and operate at frequencies up to several hundred kilohertz [16]. The increase in frequency accelerates the saturation process of the transformer, and once it reaches magnetic saturation, it will overheat, breakdown, and potentially damage the power supply. This is especially risky for non-sinusoidal magnetization excitations, as they could potentially accelerate the magnetization of the transformer to saturation and reduce its normal working range. Second, different annealing temperatures during the preparation of nanocrystalline alloys result in varying grain sizes, which affect the magnetic domain microstress inside the crystal phase, the interface microstress between the crystal phase and the amorphous phase, and the internal eddy current circuit during magnetization, ultimately affecting the core loss of the alloy. Therefore, it is essential to study the influence of nanocrystalline alloy grain size on the high-frequency magnetic loss of the material under high-frequency non-excitation.

In this article, we construct an ac test system based on the ring sample method to measure the high-frequency loss of nanocrystalline alloys under $H = 0.7$ T and $f = 10$ kHz sinusoidal alternating magnetic field excitation. Subsequently, we establish a 3-D nanocrystalline alloy model with the corresponding mesoscopic scale. The model core loss is obtained by applying the same alternating magnetic field, and the above two loss values are compared to verify the model accuracy. We then investigate the high-frequency magnetic losses of nanocrystalline alloys with different grain sizes of 6, 10, and 15 nm under sinusoidal alternating magnetic field excitation from a microscopic level by taking the grain size d as an investigation parameter. Finally, we examine the influence of d of the nanocrystalline alloy and different non-sinusoidal alternating magnetic field excitations (including square wave, trapezoidal wave, and triangular wave) on the high-frequency loss of the nanocrystalline alloy. This study provides a theoretical foundation and key technology for the design and application of new high-frequency transformer core materials.

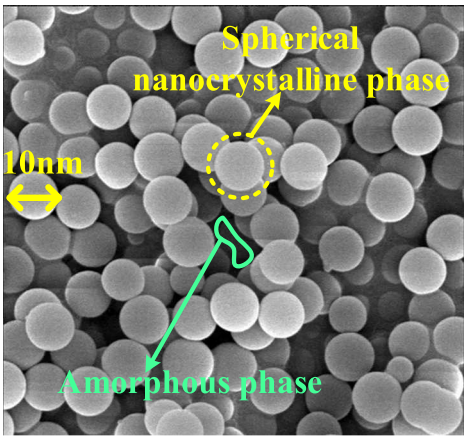

Fig. 1. Microstructure of nanocrystalline alloy.

II. Mesoscopic Model of Nanocrystalline Alloy

The Fe-based nanocrystalline soft magnetic alloy under study in this article is Finemet alloy [17], with a composition of $Fe_{73.5}Cu_1Nb_3Si_{13.5}B_9$. It is produced by the crystallization of amorphous precursors, resulting in a dual-phase structure consisting of spherical grains and amorphous phases. Due to the spherical grains' typical size of about 10 nm, it is also referred to as spherical nanocrystalline [18]. Its static characteristic parameters are as follows: static saturation magnetic field H_s is 225 kA/m, saturation magnetic flux density B_s is 1.24 T, and coercive force H_c is 310 A/m. The alloy's microstructure, as shown in Fig. 1 [19], comprises spherical nanocrystalline phases of different sizes randomly distributed on the amorphous phases, which were observed using the ZEISS-40MAT optical microscope. Moreover, the nanocrystalline alloy exhibits the best soft magnetic properties when the volume fraction of the spherical nanocrystalline phase in the material is 60%–70%.

The ferromagnetic properties of nanocrystalline alloy materials are greatly influenced by the exchange coupling between the crystalline and amorphous phases. Therefore, the following formula can be employed to determine the exchange coefficient $A_{\text{cry}-\text{Amor}}$ between the nanocrystalline crystalline phase and the amorphous phase:

$$A_{\text{cry}-\text{Amor}} = \sqrt{A_{\text{cry}} \times A_{\text{Amor}}} \tag{1}$$

where A_{cry} represents the exchange constant of crystal phase and A_{Amor} represents the exchange constant of amorphous phase.

To facilitate modeling, the nanospherical grains in the nanocrystalline alloy and the small regions in the amorphous matrix are assumed to be ferromagnetic units with a small magnetization intensity vector and an easy magnetization axis. The starting state direction is assumed to be random. The following additional assumptions are also made for the model.

1) As there is no crystal structure within the amorphous phase, the anisotropic constants can ideally be considered zero.
2) The internal structure of the material consists of nanospherical grains uniformly distributed throughout the amorphous matrix.

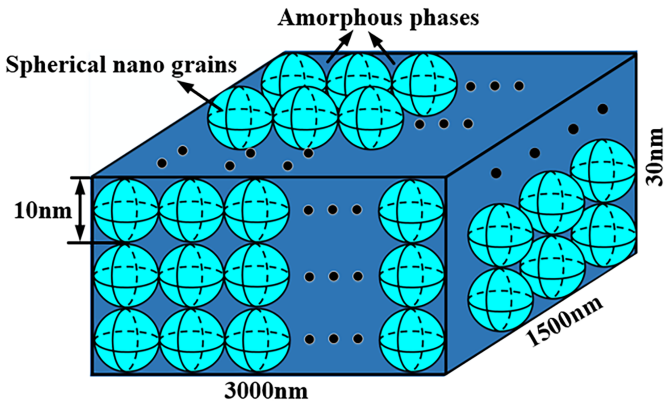

Fig. 2. Schematic of nanocrystalline alloy model.

TABLE I
SIGNIFICANT MAGNETIC PROPERTIES OF NANOCRYSTALLINE ALLOYS

	Exchange coefficient A (J/m)	Magneto crystalline anisotropy constant K_1 (J/m^3)	Saturation magnetization M_s (T)
Nanocrystalline phase	1×10^{-11}	8×10^{2}	1.31
Amorphous phase	6×10^{-12}	0	1.16

3) In the model, the nanospherical grains are arranged horizontally in parallel.

Fig. 2 illustrates a 3-D mesoscopic model of the alloy created using micromagnetic simulation software (OOMMF) based on G. Herzer's random anisotropy theory [20]. The model consists of cyan spheres representing spherical nanocrystalline grains, and dark blue regions representing the space between the grains, which corresponds to the amorphous phase observed in Fig. 1. The established model shown in Fig. 2 has an overall size of 4000 × 1500 × 30 nm, with horizontally inserted spherical nanocrystals having a diameter of 10 nm within the amorphous matrix.

Table I lists the significant magnetic parameters used during the model establishment process. Unless otherwise specified in this article, this model is utilized for simulation calculations.

III. VALIDATION OF NANOCRYSTALLINE ALLOY MICROMAGNETIC MODEL

A. Calculation of Static Characteristic Parameters of Model

To verify the accuracy of the micromagnetic model for the nanocrystalline alloy, we measured the principal direct current magnetic properties, including the static saturation magnetic field strength (H_s), saturation magnetic flux density (B_s), and coercivity (H_c), using a direct magnetic testing device. The testing apparatus, designed by the Magnetic Measurement Laboratory at the Chinese National Institute of Metrology (type: NIM-2000S), is shown in Fig. 3. The test ring has a diameter of 32 mm for the inner ring, 50 mm for the outer ring, and a thickness of 20 mm.

Finally, the main direct current magnetic properties of the nanocrystalline alloy are as follows: H_s is 225 kA/m, B_s is 1.24 T, and H_c is 310 A/m [21]. Fig. 4 shows the information about the model's static hysteresis loop when subjected to a static magnetic field ranging from −1 to +1 T.

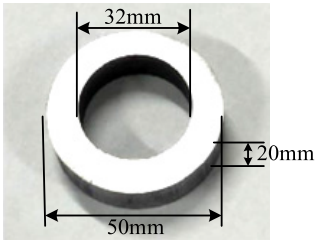

Fig. 3. Ring for magnetic testing.

TABLE II
COMPARISON OF MODEL DATA AND EXPERIMENTAL DATA OF NANOCRYSTALLINE ALLOY

	H_s (kA/m)	B_s (T)	H_c (A/m)
Model Data	210	1.247	307
Experimental Data	225	1.24	310

From Fig. 4(b), it is apparent that the nanocrystalline alloy approaches saturation when the external magnetic field reaches 210 kA/m, with B_s being 1.247 T. Additionally, Fig. 4(c) shows that when the magnetic flux density is 0, the applied magnetic field is approximately 307 A/m.

Table II compares the model data with the experimental data of the nanocrystalline alloy. The model data are obtained from the hysteresis loop of the model, while the experimental data are measured by the NIM-2000S test device. The direct current magnetic properties of the nanocrystalline alloy micromagnetic model are not significantly different from the experimental sample, as shown in Table II. Therefore, it can be concluded that the constructed micromagnetic model is reliable.

B. Measurement of Dynamic Hysteresis Loop

To further verify the accuracy of the model, this article has constructed a magnetic performance test system based on the ring sample method to measure the high-frequency magnetic loss of the nanocrystalline alloys. The test device is presented in Fig. 5.

Fig. 5 illustrates the magnetic performance test system constructed in this study, which mainly consists of an excitation module, a test module, and a data processing module. The excitation module comprises a signal source (type: UTG2025A, manufacturer: UNI-T) and a power amplifier (type: ATA-308, manufacturer: Aigtek). The signal source generates sinusoidal magnetic fields with different frequencies and amplitudes, which are amplified by the power amplifier and applied to the primary side of the test sample. The test module is composed of a test sample and a blocking capacitor. The blocking capacitor eliminates the effect of dc bias on the core loss of the nanocrystalline alloy. The voltage probe (type: TT-HVP08, manufacturer: TESTEC) is connected to the two

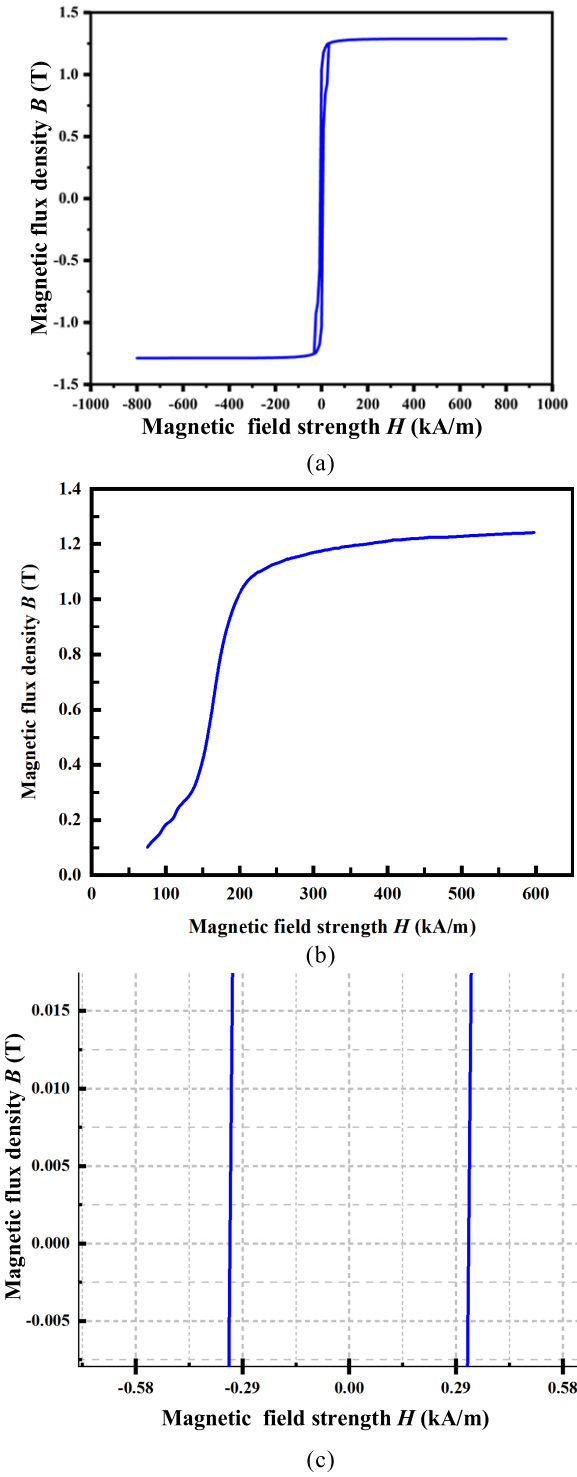

Fig. 4. Static hysteresis loop of nanocrystalline alloy. (a) Static hysteresis loop. (b) Static magnetization curve. (c) Local amplification of static hysteresis loop.

ends of the sampling resistor and the secondary side of the test sample. The oscilloscope (type: DPO5000B, manufacturer: Tektronix) is used to observe the collected data, which are then sent to the PC for further analysis.

Due to the influence of an alternating magnetic field, the repeated periodic magnetization process of ferromagnetic materials is referred to as dynamic magnetization. During

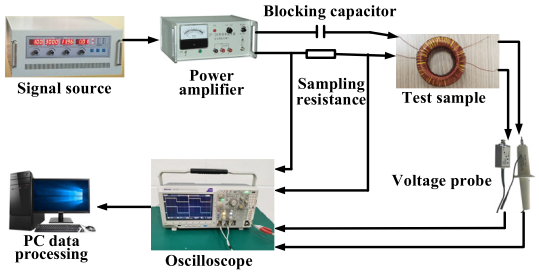

Fig. 5. Test system installation diagram.

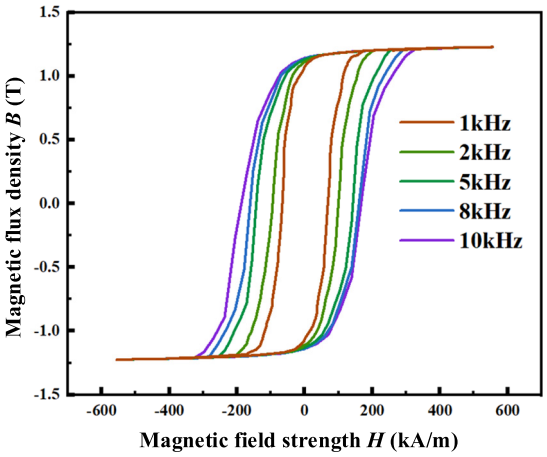

Fig. 6. Dynamic hysteresis loops of ring samples at different frequencies.

dynamic magnetization, the magnetic loss per unit volume of the ferromagnetic material magnetized for one cycle is equal to the area enclosed by the dynamic hysteresis loop [22]. To obtain the dynamic hysteresis loop and magnetic loss at different frequencies, a sinusoidal magnetic field with a maximum magnetic flux density of $B_m = 0.7$ T and frequencies ranging from 1 to 10 kHz is applied to the ring sample of nanocrystalline alloy using the alternating magnetic field test system platform shown in Fig. 5.

Fig. 6 illustrates the dynamic hysteresis loop of the ring specimen under various frequency alternating magnetic field excitations.

The figure illustrates that the dynamic hysteresis loop has a similar shape to the static hysteresis loop, but the area surrounded by the dynamic hysteresis loop is significantly larger than that of the static loop, and its shape and size also vary with the magnetic field. This is because, during the process of dynamic magnetization, the magnetic loss in the material includes not only hysteresis loss but also eddy current loss and residual loss.

To verify the accuracy of the model, a sinusoidal magnetic field with $B_m = 0.7$ T and frequency ranging from 1 to 10 kHz was applied to the established micromagnetic model to obtain its dynamic hysteresis loop. During the simulation, data were stored using the mmData Table function in the software, and a Python script was used to extract the magnetic flux density (B) and magnetic field strength (H) in the magnetization process of the nanocrystalline alloy. The dynamic hysteresis loops of the nanocrystalline alloy under various alternating magnetic

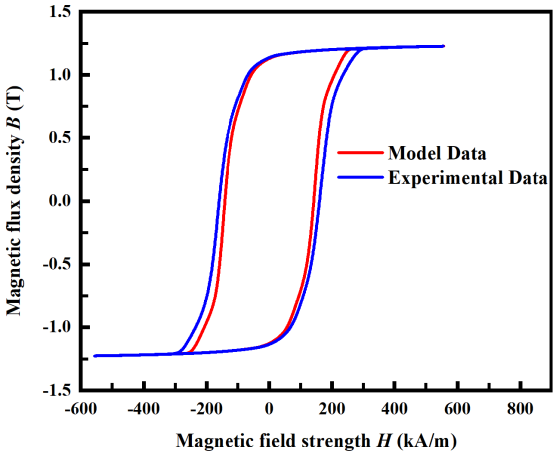

Fig. 7. Dynamic hysteresis loop of the model and test sample under 10 kHz excitation.

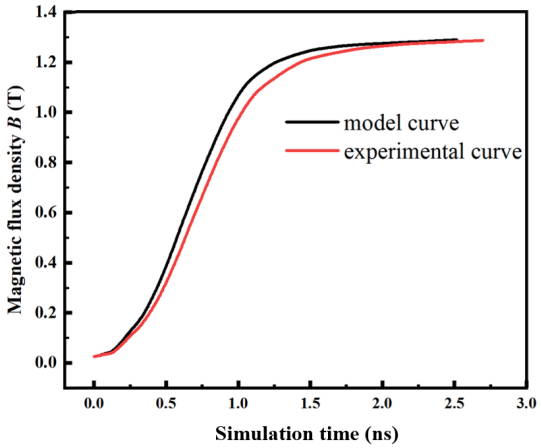

Fig. 8. Comparison of magnetization curve between model and experimental sample.

TABLE III
COMPARISON OF EXPERIMENTAL DATA AND SIMULATION DATA ON MAGNETIC LOSS OF NANOCRYSTALLINE ALLOY

	High-Frequency Loss P_v (kW/m^3)				
	1kHz	2kHz	5kHz	8kHz	10kHz
Experimental Data	7.11	15.27	51.11	100.63	140.01
Simulated Data	7.64	16.35	53.24	102.36	141.98
Difference between the two values	0.53	1.08	2.13	1.73	1.97

fields were then plotted using drawing software. The magnetic loss of the nanocrystalline alloy was obtained by calculating the area enclosed by the hysteresis loop. Fig. 7 illustrates the dynamic hysteresis loop of the model and test sample under an excitation of 10 kHz.

The loss value of the model under the excitation of 10 kHz is calculated by determining the area surrounded by the dynamic hysteresis loop in Fig. 7, resulting in a value of 141.98 kW/m^3.

Table III presents the comparison between the core loss measured experimentally and the loss obtained through simulation under various frequency excitations. The table shows that the magnetic loss obtained from the model simulation is similar to the experimentally measured magnetic loss, thereby confirming the accuracy of the model. This further demonstrates that the dynamic hysteresis loop produced by micromagnetic simulation software can be used to study the high-frequency loss of nanocrystalline alloys.

The variation curve of the magnetic flux density B over time during magnetization of the model is plotted and compared with the curve of the ring specimen, as shown in Fig. 8. Due to the presence of ferromagnetic material, the saturation magnetic flux density is greater than the maximum magnetic flux density of the external magnetic field. Fig. 8 shows that the variation curve of the model is not significantly different from the curve of the ring specimen.

IV. EFFECT OF D ON HIGH-FREQUENCY MAGNETIC LOSS

Nanocrystalline soft magnetic alloys are produced via crystallization annealing at specific temperatures, resulting in a microstructure comprising two distinct phases: a crystal phase and an amorphous phase. The crystal phase has a complex composition, mainly consisting of Fe, along with some Cu and transition element Nb. Moreover, due to varying annealing temperatures employed during material preparation, the grain size of the material varies, leading to changes in magnetic domain microstress within the crystal phase, interface microstress between the crystal phase and amorphous phase, and internal eddy current loop during magnetization, all of which ultimately affect the alloy's magnetic loss. In this study, a micromagnetic model of the nanocrystalline alloy was constructed using micromagnetic simulation software, and by altering the parameter d, the material's high-frequency magnetic loss was investigated.

When exploring the influence of d on the high-frequency magnetic loss of nanocrystalline alloy, d is set to 6, 10, and 15 nm, respectively. The model is then exposed to a sinusoidal magnetic field with f of 1–20 kHz and $B_m = 0.7$ T. In the simulation process, the data in the simulation process are stored by the mmData Table (data storage function) of the software, and then, the data are screened by Python script to obtain B and H of the material. Then, using drawing software, nanocrystalline alloy's dynamic hysteresis loop under various alternating magnetic field excitation is depicted. Finally, the area surrounded by the dynamic hysteresis loop is calculated by integral calculation, that is, the magnetic loss of nanocrystalline alloy. Fig. 9 shows the dynamic hysteresis loops of nanocrystalline alloys with different grain sizes excited at 20 kHz.

When investigating the influence of grain size d on the high-frequency magnetic loss of nanocrystalline alloys, d is set to 6, 10, and 15 nm, respectively. The model is then exposed to a sinusoidal magnetic field with a frequency range of 1–20 kHz and B_m of 0.7 T. During the simulation process, data are stored using the software's mmData Table (data storage function) and then screened using a Python script to obtain the material's B and H values. Using drawing software, the dynamic hysteresis loops of the nanocrystalline alloy under various alternating magnetic field excitations are plotted. Finally, the area surrounded by the dynamic hysteresis loop is calculated to obtain

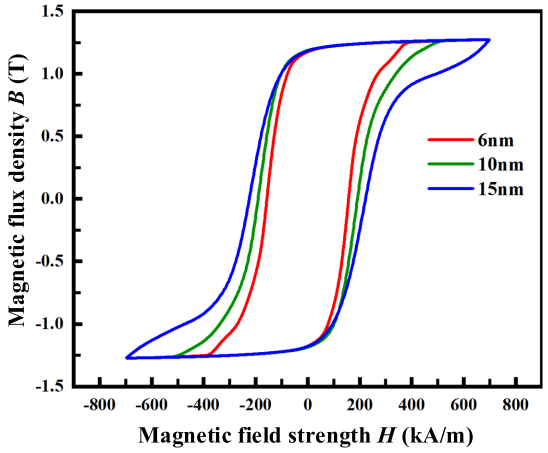

Fig. 9. Dynamic hysteresis loops of nanocrystalline alloys with different d values under 20 kHz excitation.

TABLE IV
HIGH-FREQUENCY LOSS OF NANOCRYSTALLINE ALLOY WITH DIFFERENT d VALUES

d (nm)	P_v (kW/m^3)					
	1kHz	2kHz	5kHz	8kHz	10kHz	20kHz
6	6.91	13.88	42.59	81.89	113.58	234.21
10	7.64	16.35	53.24	102.36	141.98	296.72
15	9.36	21.82	65.88	120.83	172.45	356.75

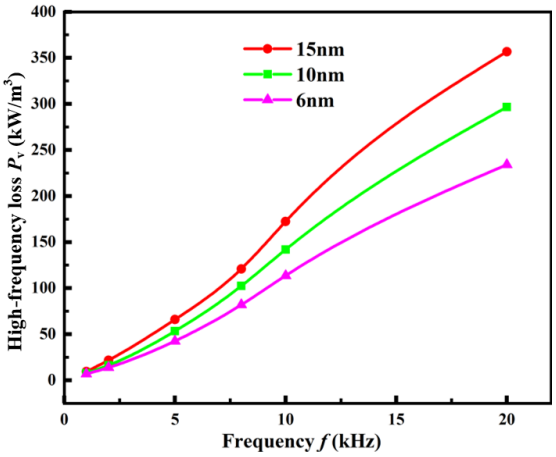

Fig. 10. Variation curve of high-frequency loss of nanocrystalline alloy with different d values.

the magnetic loss of the nanocrystalline alloy. Fig. 9 illustrates the dynamic hysteresis loops of nanocrystalline alloys with different grain sizes, excited at 20 kHz.

Based on Fig. 9, it can be observed that as the value of d increases, the area surrounded by the dynamic hysteresis loop of the nanocrystalline alloy also increases, indicating an increase in the high-frequency magnetic loss of the material. Table IV presents the high-frequency loss values of nanocrystalline alloys with d values of 6, 10, and 15 nm under 1–20 kHz excitation. A curve of high-frequency loss of nanocrystalline alloys with d was drawn based on the data in the table, as illustrated in Fig. 10.

Based on Fig. 10, it is evident that the high-frequency loss of the nanocrystalline alloy gradually increases as d increases. Furthermore, the increase in the frequency of the external magnetic field leads to a more significant increase in the high-frequency loss. Specifically, when d increases from 6 to 15 nm while $f = 1$ kHz remains constant, the magnetic loss of the nanocrystalline alloy increases from 6.91 to 9.36 kW/m^3, indicating a growth rate of 35.46%. Similarly, when d increases from 6 to 15 nm while $f = 20$ kHz remains constant, the high-frequency magnetic loss of the material increases from 234.21 to 356.75 kW/m^3, indicating a growth rate of 52.32%.

The aforementioned phenomenon can be explained by the loss separation method. The magnetic loss of ferromagnetic materials includes static and dynamic losses. The static loss, also known as hysteresis loss, is the energy loss that results from the friction generated by the internal magnetic domain rotation of ferromagnetic materials during magnetization. The dynamic loss is further divided into eddy current loss and residual loss. Compared to the eddy current and hysteresis losses, the residual loss is negligible. The expression for calculating the magnetic loss of ferromagnetic materials using the loss separation method is as follows:

$$\begin{aligned} p_v &= p_h + p_{\text{dyn}} \\ &= p_h + p_e + p_{\text{exc}} \\ &= k_h f B_m^{\lambda} + k_e f^2 B_m^2 + k_{\text{exc}} f^{1.5} B_m^{1.5} \end{aligned} \tag{2}$$

where p_v represents the core loss of ferromagnetic material in (kW/m^3), p_h represents the hysteresis loss of the ferromagnetic material, p_e represents the eddy current loss of ferromagnetic materials, p_{exc} represents the hysteresis loss of a ferromagnetic material, and λ is the Steinmetz coefficient. k_h, k_e, and k_{exc} are the coefficients for hysteresis loss, eddy current loss, and abnormal loss, respectively.

The coefficient of hysteresis loss with respect to frequency is lower than that of eddy current loss. Therefore, as the frequency increases (up to kHz), the value of eddy current loss will become much larger than that of hysteresis loss, making the hysteresis loss negligible. As a result, the high-frequency loss in this study is mainly composed of eddy current loss. Since the grain structure of ferromagnetic materials is spherical, the calculation of eddy current loss in the unit volume of the material can be determined using formula (3). For sinusoidal alternating magnetic fields, formula (3) can be simplified to the following expression [23], [24]:

$$p_e^{\text{inter}}\big|_V = \frac{d^2}{40 R_{\text{bulk}}} \left(\frac{dB}{dt}\right)^2 \tag{3}$$

$$p_e^{\text{inter}}\big|_V = \frac{(\pi d B_m)^2}{20 R_{\text{bulk}}} f^2 \tag{4}$$

where d represents the diameter of the spherical grains, measured in meters m; B represents the amplitude of the applied alternating magnetic field, measured in T; f represents the frequency of the external magnetic field, measured in Hz; R_{bulk} represents the resistivity of the material, measured in Ω·m.

The volume of crystalline phase in nanocrystalline alloy material can be expressed by the following formula:

$$V_{\mathrm{cry}} = \frac{m_{\mathrm{Nano}} V}{\rho_{\mathrm{Nano}}} \tag{5}$$

where V_{cry} represents the crystal phase volume of nanocrystalline alloys, measured in cm^3; m_{Nano} denotes the mass of the material, measured in g; ρ_{Nano} represents the density of nanocrystalline alloys, measured in $\mathrm{g/cm}^3$; V is the crystal phase volume fraction of nanocrystalline alloys.

The total eddy current loss of the material can be expressed as the product of formulas (4) and (5), yielding the following formula:

$$\begin{aligned} P_e^{\mathrm{inter}}\big|_{\mathrm{total}} &= p_e^{\mathrm{inter}}\big|_V \times V_{\mathrm{cry}} \\ &= \frac{(\pi d B_m)^2}{20 R_{\mathrm{bulk}}} f^2 \times \frac{m_{\mathrm{Nano}} V}{\rho_{\mathrm{Nano}}} \\ &= \frac{(\pi d B_m f)^2 m_{\mathrm{Nano}} V}{20 R_{\mathrm{bulk}} \rho_{\mathrm{Nano}}}. \end{aligned} \tag{6}$$

The formula above shows that as the diameter of the grains increases, the eddy current loss of the material will also increase.

V. Influence of High-Frequency Non-Sinusoidal Excitation on Magnetic Loss

High-frequency transformers encounter a range of complex operating conditions, where their excitation voltages and currents are not standard sine waves, but instead non-sinusoidal waves with a large number of harmonics. High-frequency transformers operate at frequencies up to several hundred kilohertz. As the frequency increases, the transformer's saturation process accelerates. Once the transformer becomes magnetically saturated, it can overheat, breakdown, and cause damage to the power supply. This is particularly problematic for non-sinusoidal magnetization excitation, where there is a risk of accelerating the magnetization of the transformer to saturation and reducing its normal working range. To study the effect of different non-sinusoidal alternating magnetic field excitations on the high-frequency loss of nanocrystalline alloys, this article applies the three most common non-sinusoidal waves (square wave, trapezoidal wave, and triangular wave) to the model and explores the high-frequency magnetic loss of nanocrystalline alloys under non-sinusoidal excitation.

During the simulation process, the value of d was kept constant, while the model was subjected to alternating magnetic fields of square wave, trapezoidal wave, and triangular wave with $B_m = 0.7$ T and frequency f ranging from 1 to 20 kHz.

The data processing follows similar steps as that of studying the influence of different d on the high-frequency magnetic loss. Under the excitation of three non-sinusoidal magnetic fields with $B_m = 0.7$ T and f ranging from 1 to 20 kHz, the magnetic flux density B and magnetic field strength H of the nanocrystalline alloy are measured. The dynamic hysteresis loops of different d values under three non-sinusoidal alternating magnetic fields are plotted, and the area enclosed by the dynamic hysteresis loop is then calculated through integral calculation, representing the magnetic loss of the nanocrystalline alloy.

TABLE V
High-Frequency Loss of Nanocrystalline Alloy With Different Excitation Sources. (a) $d = 6$ nm. (b) $d = 10$ nm. (c) $d = 15$ nm

(a)

Excitation Source	P_v (kW/m^3)					
	1kHz	2kHz	5kHz	8kHz	10kHz	20kHz
Square wave	5.39	13.84	46.45	91.05	126.55	327.82
Trapezoidal wave	6.42	15.21	50.46	100.67	139.86	343.37
Triangular wave	8.29	17.75	57.91	115.13	156.79	370.69

(b)

Excitation Source	P_v (kW/m^3)					
	1kHz	2kHz	5kHz	8kHz	10kHz	20kHz
Square wave	7.46	16.03	51.63	103.21	144.67	350.68
Trapezoidal wave	8.79	20.85	62.89	115.67	158.25	368.74
Triangular wave	13.43	28.14	74.53	133.67	178.54	397.25

(c)

Excitation Source	P_v (kW/m^3)					
	1kHz	2kHz	5kHz	8kHz	10kHz	20kHz
Square wave	9.56	20.46	64.21	115.34	157.21	370.48
Trapezoidal wave	11.23	26.86	74.57	129.78	174.48	389.79
Triangular wave	20.86	36.12	89.16	148.31	196.45	416.37

To further investigate the effects of various non-sinusoidal alternating magnetic fields on high-frequency losses in nanocrystalline alloys, we select the dynamic hysteresis loop of nanocrystalline alloys under 20 kHz excitation, keeping the value of d constant. The excitation sources include square waves, trapezoidal waves, and triangular waves. Fig. 11 displays the dynamic hysteresis loops of nanocrystalline alloys when excited by square waves, trapezoidal waves, and triangular waves at a frequency f of 20 kHz, with d values of 6, 10, and 15 nm, respectively.

The figure demonstrates that when the excitation source is a triangular wave, the area enclosed by the dynamic hysteresis loop of the nanocrystalline alloy is the largest, followed by trapezoidal waves and square waves. This implies that the high-frequency magnetic loss of nanocrystalline alloys is greatest under triangular wave excitation, followed by trapezoidal waves and square waves.

Table V presents the high-frequency loss values of nanocrystalline alloys with d values of 6, 10, and 15 nm under excitation frequencies ranging from 1 to 20 kHz for square waves, trapezoidal waves, and triangular waves as excitation sources. Based on the data in Table V, a plot of the high-frequency magnetic loss for the material under different

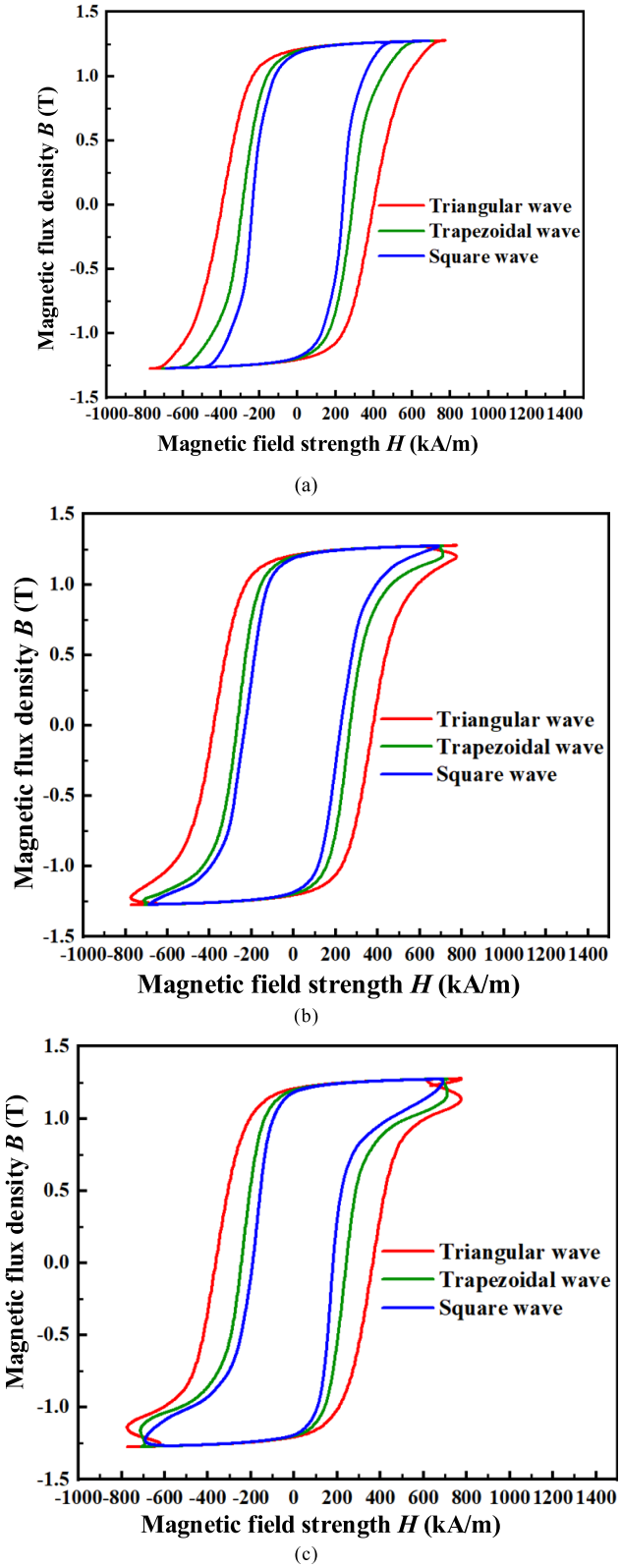

Fig. 11. Dynamic hysteresis loops of nanocrystalline alloys with different d values under 20 kHz square, trapezoidal and triangular wave excitations. (a) $d = 6$ nm. (b) $d = 10$ nm. (c) $d = 15$ nm.

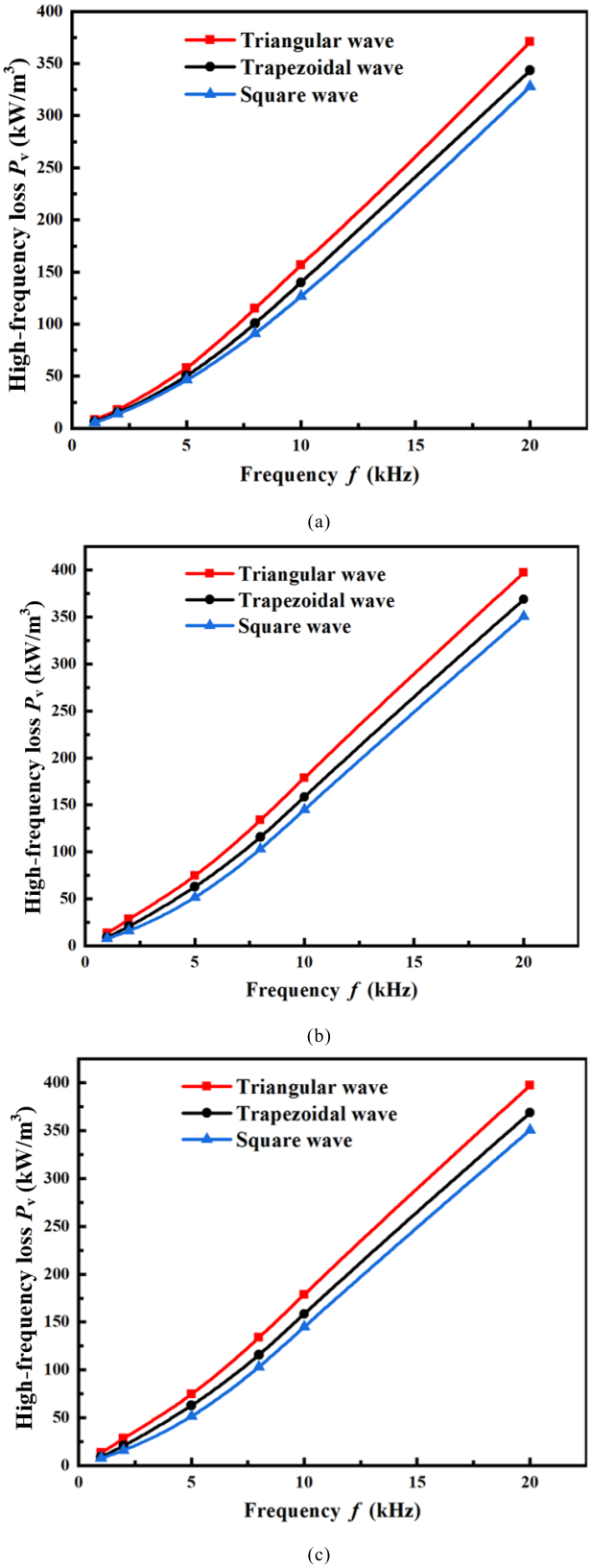

Fig. 12. High-frequency magnetic loss in nanocrystalline alloys with different d values under square wave, trapezoidal wave, and triangular wave excitation. (a) $d = 6$ nm. (b) $d = 10$ nm. (c) $d = 15$ nm.

frequency excitations of the three non-sinusoidal alternating magnetic fields is shown in Fig. 12.

As observed from these figures, when both d and f remain constant and the excitation source is a triangular wave, the high-frequency magnetic loss in nanocrystalline alloys is the highest, followed by trapezoidal waves and square waves.

When $d = 6$ nm, $f = 20$ kHz, and the excitation source is triangular wave, the high-frequency magnetic loss for the nanocrystalline alloy is 370.69 kW/m^3. With a trapezoidal wave as the excitation source, the high-frequency magnetic loss is 343.37 kW/m^3, and when the excitation source is a square wave, the high-frequency magnetic loss amounts to 327.82 kW/m^3.

When $d = 10$ nm, $f = 20$ kHz, and the excitation source is triangular wave, the high-frequency magnetic loss for the nanocrystalline alloy is 397.25 kW/m^3. With a trapezoidal wave as the excitation source, the high-frequency magnetic loss is 368.74 kW/m^3, and when the excitation source is square wave, the high-frequency magnetic loss amounts to 350.68 kW/m^3.

When $d = 15$ nm, $f = 20$ kHz, and the excitation source is triangular wave, the high-frequency magnetic loss for the nanocrystalline alloy is 416.37 kW/m^3. With a trapezoidal wave as the excitation source, the high-frequency magnetic loss is 389.79 kW/m^3, and when the excitation source is square wave, the high-frequency magnetic loss amounts to 370.48 kW/m^3.

This phenomenon can be explained by the Steinmetz formula. The Steinmetz empirical formula is the most widely used method for predicting core loss under sinusoidal excitation with high accuracy; however, this formula is not applicable for calculating core loss under non-sinusoidal excitations. As a result, Takada proposed the modified Steinmetz equation (MSE) to calculate core loss, as presented in [25]. It is believed that core loss is directly related to the magnetization rate (dM/dt), and the magnetization rate is proportional to the rate of change in magnetic flux density (dB/dt). Therefore, by using the equivalent frequency f_{eq} containing the rate of change in magnetic flux density (dB/dt) to replace the frequency f in the original Steinmetz formula, the MSE for core loss under non-sinusoidal excitations is

$$P_v = \left(K f_{\text{eq}}^{\alpha-1} B^{\beta}\right) f \tag{7}$$

where K, α, and β represent the parameters in the Steinmetz empirical formula for the same core material under sinusoidal excitation; f denotes the frequency of the non-sinusoidal excitation waveform, and f_{eq} stands for the equivalent sinusoidal magnetization frequency under non-sinusoidal excitation. The calculation for f_{eq} is as follows:

$$f_{\text{eq}} = \frac{2}{\Delta B^2 \pi^2} \int_0^T \left(\frac{dB}{dt}\right)^2 \mathrm{d}t \tag{8}$$

where ΔB represents the difference between the maximum and minimum values of magnetic flux density within a single magnetization cycle, calculated as $\Delta B = B_{\max} - B_{\min}$; $B_{\max}$ refers to the maximum magnetic flux density in one magnetization period, while $B_{\min}$ denotes the minimum magnetic flux density in the same period. When the excitation voltage does not contain a dc component, $\Delta B = 2B_m$.

For non-sinusoidal excitation waveforms, including square and triangular waves, the corresponding core loss calculation formula can be derived by following the computational process of the aforementioned correction method.

Under square wave excitation

$$u(t) = \begin{cases} U_m, & 0 \le t \le \dfrac{T}{2} \\ -U_m, & \dfrac{T}{2} \le t \le T \end{cases} \tag{9}$$

$$\Delta B = 2B_m = \frac{2}{NA_c} \int_0^{\frac{T}{4}} u dt = \frac{U_m}{2NA_c f} \tag{10}$$

$$\int_0^T \left(\frac{dB}{\mathrm{d}t}\right)^2 \mathrm{d}t = \int_0^T \left(\frac{u}{NA_c}\right)^2 \mathrm{d}t = \left(\frac{U_m}{NA_c}\right)^2 \cdot T \tag{11}$$

where N represents the number of coil turns; A_c represents the effective magnetic circuit area; U_m represents the excitation voltage amplitude. By incorporating formulas (10) and (11) into formula (8), the equivalent frequency of MSE under square wave excitation can be determined

$$f_{\text{eq}} = \frac{8}{\pi^2} \cdot f.$$

The modified Steinmetz formula under square wave excitation can be expressed as follows:

$$P_v = \left(\frac{8}{\pi^2}\right)^{\alpha-1} K f^{\alpha} B^{\beta}. \tag{12}$$

Similarly, the modified Steinmetz formula under trapezoidal wave and triangular wave excitation can be stated as follows:

$$P_v = \left(\frac{26}{3\pi^2}\right)^{\alpha-1} K f^{\alpha} B^{\beta} \tag{13}$$

$$P_v = \left(\frac{32}{3\pi^2}\right)^{\alpha-1} K f^{\alpha} B^{\beta}. \tag{14}$$

Based on formulas (12)–(14), it is clear that when K, α, and β remain constant, f_{eq} reaches its maximum value under triangular excitation, followed by trapezoidal wave excitation, and reaches its minimum value under square wave excitation. As a result, the high-frequency loss of nanocrystalline alloys is most significant under triangular excitation, followed by trapezoidal wave excitation, and is least pronounced under square wave excitation.

VI. Conclusion

To investigate the effect of grain size d and high-frequency non-sinusoidal excitation on the magnetic loss of nanocrystalline alloys, this study utilized the ring sample method to construct an ac test system that measured high-frequency loss of nanocrystalline alloys under $B_m = 0.7$ T and $f = 10$ kHz sinusoidal alternating magnetic field excitation. A 3-D model of the nanocrystalline alloy at the corresponding mesoscopic scale was then established, and by applying the same sinusoidal alternating magnetic field, the high-frequency magnetic loss of the model was obtained and compared to the previously measured loss value to verify the model's correctness. Using d as the research parameter, this study investigated the high-frequency magnetic losses of nanocrystalline alloys with d values of 6, 10, and 15 nm under sinusoidal alternating magnetic field excitation from the microscopic level. Finally, this study investigated the high-frequency magnetic loss of nanocrystalline alloys under non-sinusoidal excitation

by applying non-sinusoidal alternating magnetic fields, including square wave, trapezoidal wave, and triangular wave. The following are the main conclusions obtained in this article.

1) *Grain Size d:* As the grain size d increases, the high-frequency loss of the material also increases. Additionally, as the frequency f increases, the loss increases even more significantly. Specifically, when d increases from 6 to 15 nm while f remains at 1 kHz, the high-frequency loss of the material increases from 6.91 to 9.36 kW/m^3, showing a growth rate of 35.46%. When d increases from 6 to 15 nm while f remains at 20 kHz, the high-frequency magnetic loss of the material increases from 234.21 to 356.75 kW/m^3, indicating a growth rate of 52.32%. This can be attributed to the fact that the high-frequency loss of the material is mainly composed of eddy current loss. Since the eddy current loss of the material is positively correlated with d, an increase in d leads to a corresponding increase in the high-frequency loss of the material. This finding suggests that the eddy current loss of nanocrystalline alloy will increase with an increase in d.
2) *High-Frequency Non-Sinusoidal Excitation:* The model was subjected to three most common non-sinusoidal waves: square wave, trapezoidal wave, and triangular wave. Results showed that under unchanged values of d and f, the high-frequency magnetic loss of the material was largest when subjected to triangular wave, followed by trapezoidal wave and square wave. Specifically, when $d = 6$ nm, $f = 20$ kHz, and the excitation source was triangular wave, the high-frequency magnetic loss of the material was 370.69 kW/m^3; for trapezoidal wave, it was 343.37 kW/m^3; and for square wave, it was 327.82 kW/m^3. This was attributed to the non-sinusoidal excitation of the external magnetic field. To accurately predict the high-frequency loss of the material, the frequency equivalent f_{eq}, which contained the change rate of magnetic flux density dB/dt, could be used to replace f in the original Steinmetz formula. Calculation showed that f_{eq} was the largest under triangular excitation, followed by trapezoidal wave, and the smallest under square wave. Therefore, the high-frequency loss of nanocrystalline alloys was largest under triangular excitation, followed by trapezoidal wave, and the smallest under square excitation.

ACKNOWLEDGMENT

This work was supported in part by the National Natural Science Foundation of China under Grant 51977122 and in part by the State Key Laboratory of Reliability and Intelligence of Electrical Equipment under Grant EERI_KF2021011.

REFERENCES

[1] E. A. Theisen, "Recent advances and remaining challenges in manufacturing of amorphous and nanocrystalline alloys," *IEEE Trans. Magn.*, vol. 58, no. 8, pp. 1–7, Aug. 2022.

[2] H. Kumaoka, A. Hasegawa, S. Mori, K. Horino, and H. Matsumoto, "Fe-B-Nb-P nanocrystalline alloy with high amorphous forming ability for fabricating the powder," *IEEE Trans. Magn.*, vol. 56, no. 4, pp. 1–4, Apr. 2020.

[3] W. Zhang, Q. Yang, Y. Li, Z. Lin, M. Yang, and M. Mi, "Comprehensive analysis of nanocrystalline ribbon cores in high-power-density wireless power transfer pads for electric vehicles," *IEEE Trans. Magn.*, vol. 58, no. 2, pp. 1–5, Feb. 2022.

[4] X. Chen et al., "Microstructure and magnetic properties evolution of isotropic nanocrystalline NdFeB hot-pressed magnets with CeCu addition," *IEEE Trans. Magn.*, vol. 57, no. 12, pp. 1–6, Dec. 2021.

[5] P. Cao, Y. Liu, J. Li, J. Du, R. Wang, and T. Zhou, "Enhanced magnetic properties of hot-pressed Fe-based nanocrystalline powder cores with low-melted glass-modified insulating," *IEEE Trans. Magn.*, vol. 57, no. 4, pp. 1–7, Apr. 2021.

[6] L. Yongjian et al., "Numerical prediction of losses and local overheating in transformer windings based in magnetic-thermal-fluid model," *Trans. China Electrotechnical Soc.*, vol. 35, no. 21, pp. 4483–4491, 2020.

[7] Y. Hua et al., "Effect of Co content on microstructures and magnetic properties of anisotropic bulk $TbCu_7$-type Sm-Co nanocrystalline magnets," *IEEE Trans. Magn.*, vol. 56, no. 1, pp. 1–4, Dec. 2020.

[8] Y. Jianxin and L. Yongjian, "Characteristics and developments of advanced magnetic materials in electrical engineering: A review," *Trans. China Electrotechnical Soc.*, vol. 31, no. 20, pp. 1–12, 2016.

[9] J. Füzer, S. Dobák, and P. Kollár, "Magnetization dynamics of FeCuNbSiB soft magnetic ribbons and derived powder cores," *J. Alloys Compounds*, vol. 628, pp. 335–342, Apr. 2015.

[10] A. Bachleitner-Hofmann, B. Bergmair, T. Schrefl, A. Satz, and D. Suess, "Soft magnetic properties of thin nanocrystalline particles due to the interplay of random and coherent anisotropies," *IEEE Trans. Magn.*, vol. 53, no. 11, pp. 1–6, Apr. 2017.

[11] Y. N. Starodubtsev, V. A. Kataev, K. O. Bessonova, and V. S. Tsepelev, "Hysteresis losses in nanocrystalline alloys with magnetic-field-induced anisotropy," *J. Magn. Magn. Mater.*, vol. 479, pp. 19–26, Jun. 2019.

[12] Z. Zhang, X. Liu, S. Feng, J. Tang, and M. Shezad, "The glass formation ability and soft magnetic properties of the $Fe_{79}Si_9B_{4.5}P_{1.5}CuNb_x$ nanocrystalline alloys," *J. Magn. Magn. Mater.*, vol. 497, Mar. 2020, Art. no. 165990.

[13] D. Kampen, M. Owzareck, S. Beyer, N. Parspour, and S. Schmitt, "Analytical core loss models for electrical steel in power electronic applications," in *Proc. 13th Int. Conf. Optim. Electr. Electron. Equip. (OPTIM)*, May 2012, pp. 109–117.

[14] W. Jiale, "Micromagnetic simulation od high frequency saturation mechanism for nanocrystalline alloy in mesoscopic scale," M.S. dissertation, Shandong Univ., Jinan, China, 2018.

[15] H. Zhiyun et al., "Micromagnetic analysis of external and internal impact factors on kHz level saturation magnetization for nanocrystalline alloy," *Trans. China Electrotechnical Soc.*, vol. 34, no. 8, pp. 1589–1598, 2019.

[16] C. Bin, L. Lin, and Z. Zhibin, "Loss and magnetic core loss in dual-active-bridge DC–DC converter," *Trans. China Electrotechnical Soc.*, vol. 32, no. 22, pp. 123–133, 2017.

[17] Y. Yoshizawa, S. Oguma, and K. Yamauchi, "New Fe-based soft magnetic alloys composed of ultrafine grain structure," *J. Appl. Phys.*, vol. 64, no. 10, pp. 6044–6046, 1988.

[18] M. A. Willard et al., "Structure and magnetic properties of $(Fe_{0.5}Co_{0.5})_{88}Zr_7B_4Cu_1$ nanocrystalline alloys," *J. Appl. Phys.*, vol. 84, no. 12, pp. 6773–6777, Dec. 1998.

[19] T. Li, Y. Li, L. Wu, L. Qi, and W. Zhang, "Improvement of soft magnetic properties of a $Fe_{84}Nb_7B_9$ nanocrystalline alloy by synergistic substitution of P and Hf," *J. Alloys Compounds*, vol. 918, Oct. 2022, Art. no. 165735.

[20] G. Herzer, "Grain size dependence of coercivity and permeability in nanocrystalline ferromagnets," *IEEE Trans. Magn.*, vol. 26, no. 5, pp. 1397–1402, 1990.

[21] Z. Zhenghan, "Research on high-frequency transformer's magnetic core and winding characteristic in power electronic transformer," Ph.D. dissertation, Hebei Univ. Technol., Tianjin, China, 2014.

[22] Z. Qing, "Predicting core loss of amorphous nanocrystalline materials under complex excitation," Ph.D. dissertation, Hebei Univ. Technol., Tianjin, China, 2017.

[23] A. H. Taghvaei, H. Shokrollahi, K. Janghorban, and H. Abiri, "Eddy current and total power loss separation in the iron–phosphate–polyepoxy soft magnetic composites," *Mater. Design*, vol. 30, no. 10, pp. 3989–3995, Dec. 2009.

[24] A. H. Taghvaei, A. Ebrahimi, K. Gheisari, and K. Janghorban, "Analysis of the magnetic losses in iron-based soft magnetic composites with MgO insulation produced by sol–gel method," *J. Magn. Magn. Mater.*, vol. 322, no. 23, pp. 3748–3754, Dec. 2010.

[25] J. Reinert, A. Brockmeyer, and R. W. A. A. De Doncker, "Calculation of losses in ferro- and ferrimagnetic materials based on the modified Steinmetz equation," *IEEE Trans. Ind. Appl.*, vol. 37, no. 4, pp. 1055–1061, Jul./Aug. 2001.

Li Zhang (Member, IEEE) received the B.Sc., M.Sc., and Ph.D. degrees from the School of Electrical Engineering, Shandong University, Jinan, China, in 2001, 2005, and 2009, respectively.

He is currently an Associate Professor with the School of Electrical Engineering, Shandong University, with a broad research interest covering power systems electromagnetic compatibility, applied electromagnetics, and reliability analysis of electrical equipment.

Yifan Wang was born in Puyang, Henan, China, in 2000. She received the B.S. degree in electrical engineering and automation from Chang'an University, Xi'an, China, in 2022.

Her research interests include high voltage and insulation technology, high-frequency power electronic transformers, and materials of various electromagnetic equipments.

Liang Zou (Member, IEEE) received the B.Sc., M.Sc., and Ph.D. degrees from the School of Electrical Engineering, Shandong University, Jinan, China, in 2004, 2007, and 2011, respectively.

He is currently a Professor with the School of Electrical Engineering, Shandong University. He is devoted to the research with a broad research interest covering high voltage and insulation, applied electromagnetics, and high-frequency transformer.

Kaihang Guo was born in Taiyuan, Shanxi, China, in 1997. He received the master's degree from the School of Electrical Engineering, Shandong University, Jinan, China, in 2023.

After graduation, he worked with Dalian Power Supply Company of State Grid Liaoning Electric Power Company Ltd. His research interests include high voltage and insulation technology, applied electromagnetism, and materials of various electromagnetic equipments especially for high-frequency power electronic transformers.

Yongjian Li was a Research Assistant with the University of Technology Sydney (UTS), Ultimo, NSW, Australia, from 2009 to 2011. He was a Visiting Scholar with Ottawa University, Ottawa, ON, Canada, from 2016 to 2017. Since 2015, he has been a Full Professor with the Electrical Engineering School, Hebei University of Technology, Tianjin, China, where he is currently the Associate Dean. His research interests include computational electromagnetics and measurements and modeling of magnetic properties.

Prof. Li is a member of International COMPUMAG Society and a Board Member of the International Steering Committee of 1&2-Dimensional Magnetic Measurement and Testing Workshop.

Qiuxia Sun received the B.Sc. degree from the School of Electrical Engineering, Shandong University, Jinan, China, in 2004, and the M.Sc. degree from the School of Electrical Engineering, Harbin Institute of Technology, Harbin, China, in 2006.

She is currently the Deputy General Manager with Shandong Taikai Transformer Company Ltd., Taian, China, mainly responsible for the research and development of new products and ultrahigh-voltage transformers.